

Authigenic Mg-Calcite at a Cold Methane Seep Site in the Laptev Sea

M. D. Kravchishina^{a,*}, A. Yu. Lein^{a,**}, A. S. Savvichev^{b,***}, L. E. Reykhard^a,
O. M. Dara^a, and M. V. Flint^a

^a*Shirshov Institute of Oceanology, Russian Academy of Sciences, Moscow, Russia*

^b*Winogradsky Institute of Microbiology, Russian Academy of Sciences, Federal Research Center Fundamentals of Biotechnology, Russian Academy of Sciences, Moscow, Russia*

**e-mail: kravchishina@ocean.ru*

***e-mail: lein@ocean.ru*

****e-mail: savvichev@mail.ru*

Received June 17, 2016

Abstract—Authigenic minerals were studied in Holocene shelf sediments of the Laptev Sea (cold methane seep site, water depth 71 m). The study presents the first finds of large hard carbonate concretions with Mg-calcite cement in recent sediments of the Arctic shelf seas. These concretions differ from previously reported glendonites and concretions from bottom sediments of the White Sea, Kara Sea, Sea of Okhotsk, etc. A study of the morphology, microstructure, and composition of these newly reported concretions revealed the multistage formation of carbonates (structural varieties of Mg-calcite and aragonite). It was shown that organic matter played an important role in the formation of authigenic carbonates, i.e., in the formation of sedimentary–diagenetic Mg-calcite. The role of methane as a possible source for authigenic carbonate formation was estimated. It was found that methane-derived Mg-calcite accounts for 17–35% of concretion materials. Mg-calcite had $\delta^{13}\text{C-C}_{\text{carb}}$ values between -24 and -23‰ and $\delta^{13}\text{C-C}_{\text{org}}$ values between -44.5 and -88.5‰ .

DOI: 10.1134/S0001437017010064

INTRODUCTION

Authigenic minerals are important indicators of physicochemical and biogeochemical deposition conditions in a marine environment. Authigenic carbonate buildups are widespread in seas and oceans around the world [7]. Two basic types of authigenic carbonates are recognized depending on the source of CO_2 : carbonates with carbon dioxide derived from anaerobic microbial decomposition of organic matter in sediments (type I), and carbonates with carbon dioxide produced by microbial oxidation of methane of any genesis (type II).

It should be noted that in both cases carbon dioxide is formed by microbial processes that lead to fractionation of carbon isotopes.

The polar seas have become a subject of growing interest in recent years because of their geographic location, discovery of new hydrocarbon accumulations in bottom sediments, and the impacts of global climate change in the Arctic region.

Since low water temperatures in the polar seas increase CO_2 solubility, carbonates are nearly absent in Quaternary bottom sediments as opposed to marine sediments in humid and arid regions.

The discoveries of authigenic carbonates derived from oxidized methane provide important evidence for the reconstruction of the depositional environment, because they carry the original carbon isotope signature of methane and can thus serve as reliable proxies for both ancient and recent methane sources.

Type I carbonate buildups include White Sea hornlets, which have long been encountered by fishermen in White Sea sediments [3, 5], as well as carbonate crusts and dendritic concretions (Fig. 1a) in Kara Sea sediments [2, 9, 10].

Type II carbonate buildups derived from methane were reported much later than the first finds of hornlet-type concretions [26]. Type II authigenic carbonates in the polar seas are represented by drusy ikaite crystals and pseudomorphs after ikaite.

Ikaite was first described by Pauly [21] at the bottom of the Ikka Fjord. Ikaite is a metastable hexahydrate of calcium carbonate ($\text{CaCO}_3 \cdot 6\text{H}_2\text{O}$). Interestingly, this mineral can crystallize in marine sediments only at low temperatures close to 0°C but rapidly decomposes into calcite and water at temperatures above 4°C . Due to its stability only at near-freezing temperatures, ancient ikaite is found decomposed into calcite pseudomorphs, known in the literature as glendonite (or gennoishi), hornlets, etc. [5].

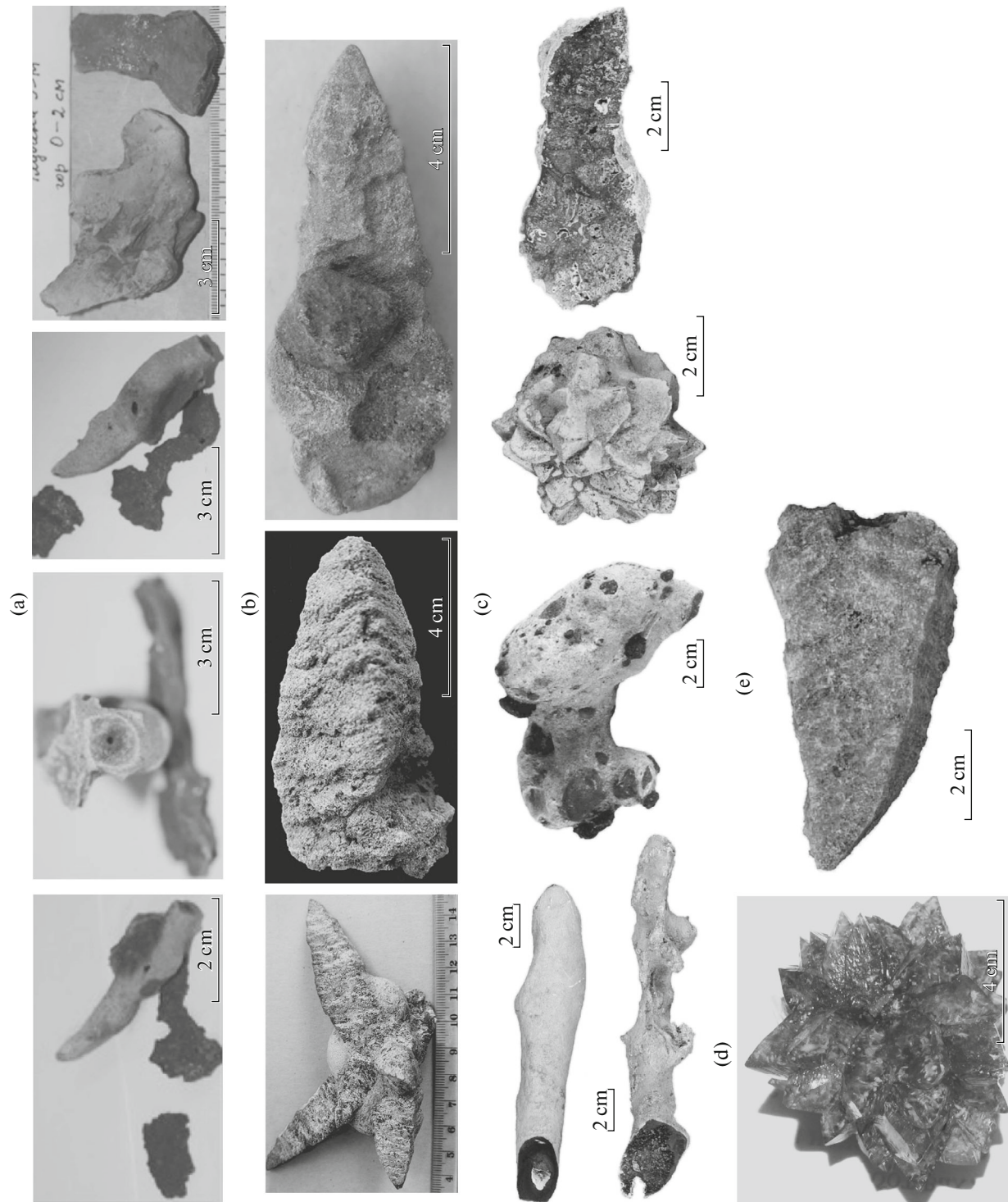


Fig. 1. Images of carbonate concretions and ikaite from bottom sediments Arctic seas: (a) concretions on surface sediments from the Kara Sea [9]; (b) glendonites from sediments of the White Sea [3]; (c) glendonites from sediments of the Sea of Okhotsk [17]; (d) ikaite druse from sediments of the Laptev Sea [6]; (e) ikaite crystal from sediments of the Sea of Okhotsk [17].

Since 1963, other significant new finds of ikaite and glendonite have been also documented in shelf sediments of Alaska [23], the Kara Sea [4, 9, 18, 19], Laptev Sea [6, 22], Sea of Okhotsk [17] and other marine environments (Fig. 1).

It should be noted that all ikaite occurrences, except for those previously reported from the Ikka Fjord, where they form high (up to 5 m) buildups, have been found not in recent surface sediments but in Holocene and even Upper Pleistocene sediments bur-

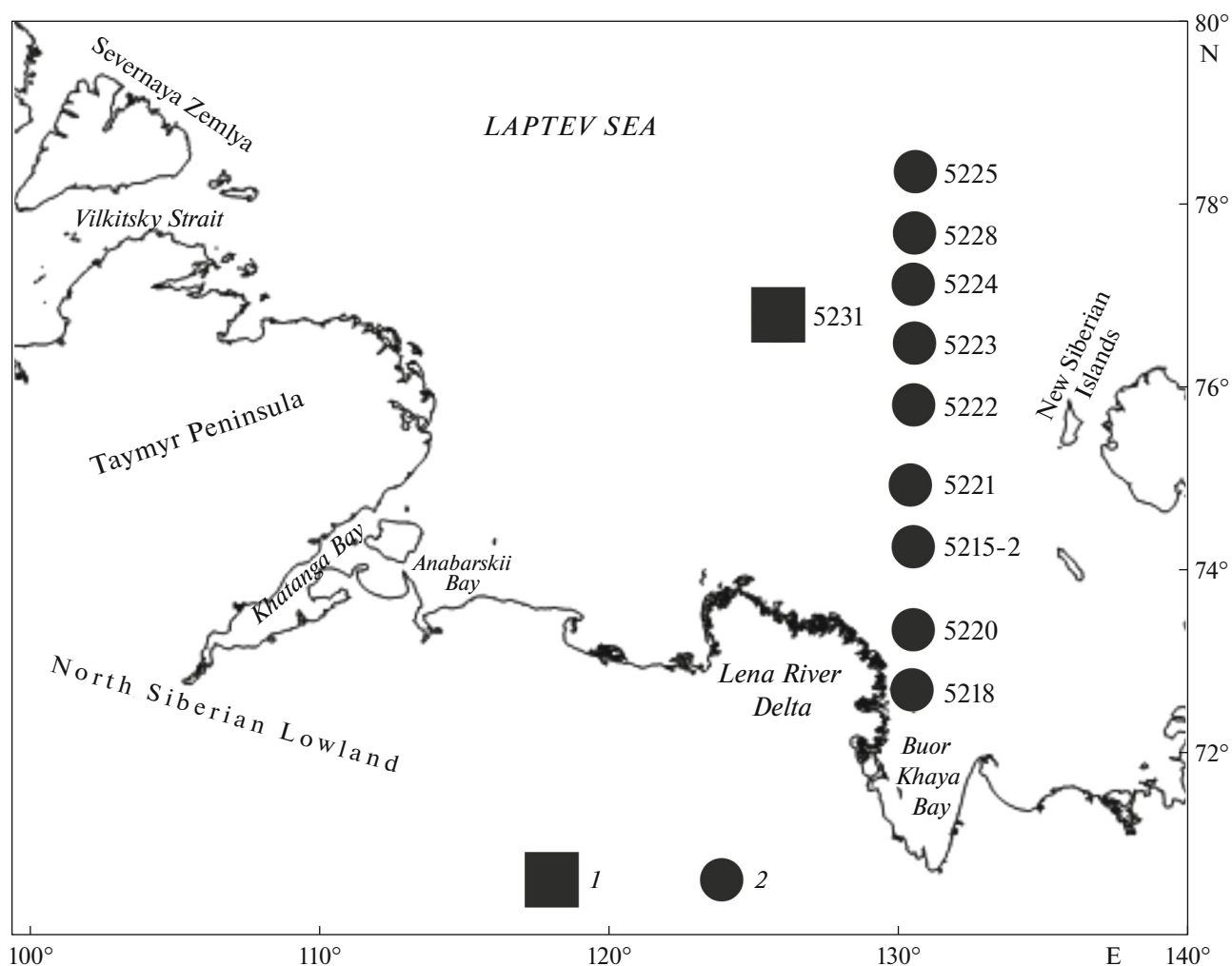


Fig. 2. Schematic map of sediment sampling sites in the Laptev Sea during cruise 63 of R/V *Akademik Mstislav Keldysh* (September–October 2016): 1—location of methane seep site, 2—station location and number.

ied at great depths below the seafloor: at a 232–238 cm sediment depth in the upper part of the continental slope at a water depth of 204 m [22], at a 150–280 cm core depth from the continental margin of the Laptev Sea at a shallow water depth of 8–18 m [6], and between a 135 and 320 cm core depth from the margin of the Kara Sea at a water depth of 87 m [2].

Previous studies show that all ikaite crystals and pseudomorphs after ikaite have light carbon isotopic signatures (from -25 to -60‰), indicating derivation from oxidation of methane [7, 8].

The first carbonate concretions consisting of Mg-calcite, rarely Mg-calcite and aragonite (Fig. 2), were recovered from a 0.5-m surface sediment layer at a $\sim 50 \times 50$ m cold methane seep in the Laptev Sea at a water depth of 71 m ($76^{\circ}46.34' \text{ N}$, $125^{\circ}49.75' \text{ E}$) during the cruise 63 of the R/V *Akademik Mstislav Keldysh* in 2015. Despite high concentrations of methane within the sediment and water column associated with low water temperatures near the sea bottom (-1.3°C), no ikaite and glendonite crystals

and druses were found in the sampled interval at the site of the cold methane seep.

Unlike ikaite crystals, carbonate concretions consisting of Mg-calcite were reported earlier in surface sediments (0–50 cm) of the Kara Sea with background methane concentrations [2, 9].

Our data and data from the literature indicate that authigenic carbonates, mostly Mg-calcite and, more rarely, aragonite were found in recent sediments of the Arctic seas with background methane concentrations, whereas ikaite and products of its pseudomorphic transformation at temperatures above $4\text{--}6^{\circ}\text{C}$ were found in sediments with anomalously high methane concentrations.

The goal of this study was to identify possible sources of carbonate (C_{carb}) and organic (C_{org}) carbon in authigenic Mg-calcite (and aragonite) from sediments with anomalously high methane concentrations using the cold methane seep site on the Laptev Sea shelf as an example.

MATERIALS AND METHODS

Samples of suspended particulate matter (SPM) were collected using a rosette SBE 32 with 6-L bottles (Bt). The sampling layers were selected based on the results of hydrophysical (Seabird SBE 911plus CTD) and hydro-optical (PUM transmissometer, Shirshov Institute of Oceanology, Russian Academy of Sciences) sensing. In order to determine the C_{org} and C_{carb} content in SPM and their isotopic composition ($\delta^{13}\text{C}-C_{\text{org}}$, $\delta^{13}\text{C}-C_{\text{carb}}$), the samples were filtered under vacuum (200 mbar) through 47-mm Whatman GF/F glass microfiber filters (0.7 μm nominal pore size).

Bottom sediments sampling was performed with a box corer (BC), Neymiste tube (NT, 1 m long, 40 mm in diameter) and a large-diameter geological gravity corer (GC, 8 m long, 110 mm in diameter). Studied materials include eight core samples about 30 cm long collected with a Neymiste tube, two gravity core samples up to 49 cm long, and two subcores taken from a 21-cm-long box corer.

The lithology was described and samples prepared according to the procedure adapted at the Shirshov Institute of Oceanology, Russian Academy of Sciences [11]. Sediment types were classified according to Bezrukov and Lisitzin's classification of marine sediments of [1]. The color of sediments samples was determined from Munsell soil color charts, 2012. The pore water in the sediment cores was removed on board [16].

The composition, texture, structure, and microtexture of carbonate concretions were studied at the Shirshov Institute of Oceanology, Russian Academy of Sciences, with a variety of methods, including standard microscopic examination of lithological thin sections using a POLAM L-213M polarizing microscope equipped with an TS-300 digital camera; scanning electron microscopy of freshly broken core chips using a VEGA-3sem TESCAN (Czech Republic) scanning electron microscope with an Oxford INCA Energy 350 electron microprobe (United Kingdom, analyst A.G. Boev); X-ray powder diffraction using a Bruker D8 Advance system (BRUKER AXC, Germany). The chemical composition of carbonate concretions was analyzed by X-ray fluorescence.

The concentration of C_{org} and C_{carb} was measured coulometrically on an AN 7560 carbon analyzer at the Shirshov Institute of Oceanology, Russian Academy of Sciences (analyst L.V. Demina). For a concentration of 30–100 $\mu\text{g C/L}$, the accuracy is $\pm 15\%$; the measurement limits are 5–500 $\mu\text{g C/L}$.

The carbon isotopic composition of CH_4 , C_{org} , and C_{carb} in bottom sediments and carbonate concretions was measured (after standard sample preparation) with a Delta Plus mass spectrometer (Germany) using the PDB standard at the Winogradsky Institute of Microbiology, Russian Academy of Sci-

ences (analyst T.S. Prusakova). The standard deviation was $\pm 0.2\%$.

The CH_4 concentration was determined by phase equilibrium degassing and subsequent gas chromatography at the Winogradsky Institute of Microbiology, Russian Academy of Sciences, using a Kristal-200-OM gas chromatograph equipped with a flame-ionization detector.

Host muds surrounding carbonate concretions were studied through a set of short-term experiments (12–48 h) when determining the rates of microbial processes, such as dark CO_2 assimilation (DAC), sulfate reduction (SR), and methane oxidation (MO) using radiotracers ($\text{NaH}^{14}\text{CO}_3$, $^{14}\text{CH}_4$, $\text{Na}_2^{35}\text{SO}_4$) under near in situ conditions [13]. Data processing in radiotracer experiments was performed by I.I. Rusanov (Winogradsky Institute of Microbiology, Russian Academy of Sciences).

The hydrochemical parameters (alkalinity, pH, O_2 , Si, and PO_4^{3-}) of water were determined as per approved guidelines for chemical analysis [13].

RESULTS

Water column profiles measured at the cold seep site (Table 1) and at background stations (5223 and 5224) show considerable variation in temperature, salinity, total alkalinity, methane concentration, and C_{org} isotopic composition of SPM [15]. The carbon isotopic composition of bicarbonate ion (HCO_3^-) in the water column at the seep site (st. 5231) varied from 0.6 to 2.9‰, which is typical of HCO_3^- in seawater and close to the background values (Table 1, Fig. 3a).

The concentration of SPM at the cold seep site varied from 0.2 mg/L near the surface to 0.7 mg/L near the bottom. The $\delta^{13}\text{C}-C_{\text{org}}$ values of SPM measured at background stations at 56–57 m water depths in the vicinity of the seep site varied from -25.5 to -32.8% (Table 1). The light isotopic composition of C_{org} in SPM from both near-surface and near-bottom water layers is caused by the contribution of light carbon derived from riverine organic matter. Lighter organic carbon isotopic values of SPM from the water column at the seep site (from -31.9 to -35.9%) (Fig. 3b) are probably due to the presence of microbial metabolites in SPM produced by methane-oxidizing bacteria (Table 1).

Host sediments. In the Laptev Sea, abundant carbonate crusts and dendritic carbonate concretions were encountered in shelf sediments within the seep site (water depth 71 m); they collected with a large-diameter gravity corer (GC-1, 0–49 cm sediment core; GC-2, 0–25 cm sediment core) and Neymiste tubes (NT) (Fig. 4). The host sediments are visibly reduced (Eh ranging from -100 to -120 mV), as identified by the presence of very dark grey to black, adhesive fine silt mud (and, more rarely, coarse silt) with indistinct lay-

Table 1. Characterization of water column and SPM at seep site and background stations, September 2015

Station Depth, m	Layer, m	Sampling tool	T, °C	S, psu	O ₂ , mL/L	pH	Alk, mg eq/L	PO ₄ ³⁻ , μM	Si, μM	CH ₄ , μL/L	δ ¹³ C-HCO ₃ ⁻ , ‰	SPM, mg/L	C _{org} , % suspension	δ ¹³ C-C _{org} , ‰	
Methane seep site 71	0.01	NT	—	—	6.08	7.79	2.421	0.48	8.38	—	—	20.56	2.0	—	
	0.1		—	—	6.14	7.83	2.456	0.42	7.47	—	—	—	—	—	
	0.2		-1.28	34.18	6.21	7.79	2.492	0.45	7.42	32.20	—	7.70	2.8	-36.6	
	-70	Bt	-1.29	34.18	6.10	7.88	2.324	0.54	7.98	7.17	2.02	0.67	2.6	-34.9	
	-60		-1.26	34.18	6.22	7.90	2.324	0.51	7.32	11.14	2.89	—	—	-35.9	
	-55		-1.28	34.00	6.23	7.94	2.317	0.67	7.02	11.64	0.56	0.48	4.2	-34.8	
	-45		-1.56	33.90	6.38	7.93	2.317	0.63	7.82	33.71	—	—	—	-32.6	
	-26		-1.18	33.43	7.27	7.99	2.310	0.57	4.97	2.98	—	—	—	-32.8	
	-12		2.68	29.02	—	—	—	—	—	—	—	—	0.15	25.3	—
	-8		2.88	27.88	—	7.99	2.118	0.26	7.17	1.64	—	—	0.21	19.0	-32.1
-2		2.99	27.42	—	—	—	—	—	1.23	—	—	—	—	—	
-1		2.97	27.38	—	—	—	—	—	—	—	1.97	0.19	12.1	-31.9	
st. 5224 60	0.02	NT	—	—	5.89	7.72	2.385	0.51	7.42	—	—	—	—	—	
	0.1		—	—	5.1	7.72	2.385	0.49	7.27	—	—	—	—	—	
	0.2		—	—	5.9	7.72	2.456	0.48	7.12	—	—	41.15	0.8	-27.7	
	0.4		-1.51	34.00	6.12	7.7	2.421	0.42	6.92	0.70	—	—	—	—	
st. 5223 55	-56	Bt	-1.51	34.01	6.63	7.84	2.317	0.46	7.02	0.63	—	1.33	2.3	-29.2	
	-35		-1.65	33.92	6.41	7.84	2.317	0.40	6.87	—	—	0.26	10.6	—	
	-2		3.56	22.57	7.68	7.94	1.876	0.09	16.55	0.94	—	0.34	9.6	-28.3	
	-0		3.57	22.02	7.43	7.89	1.834	0.10	18.16	—	—	0.60	—	—	
st. 5223 55	0.02	NT	—	—	7.2	7.74	2.421	0.51	7.77	—	—	—	—	—	
	0.1		—	—	5.84	7.73	2.385	0.49	7.57	—	—	—	—	—	
	0.2		—	—	4.46	7.71	2.385	0.51	7.47	—	—	—	—	—	
	0.4		-1.73	33.85	5.73	7.71	2.421	0.45	7.42	0.47	—	22.97	4.2	-28.8	
st. 5223 55	-53	Bt	-1.73	33.85	6.99	7.79	2.317	0.45	7.42	0.40	3.52	1.7	1.2	-30.9	
	-22		-1.28	33.28	8.01	7.91	2.281	0.23	2.11	—	—	0.20	—	—	
	-0.5		3.68	20.61	7.44	7.85	1.720	0.12	22.82	0.18	-2.62	0.28	18.0	-29.0	

Data on pH, alkalinity, O₂, phosphate and silicon concentrations are from [14].

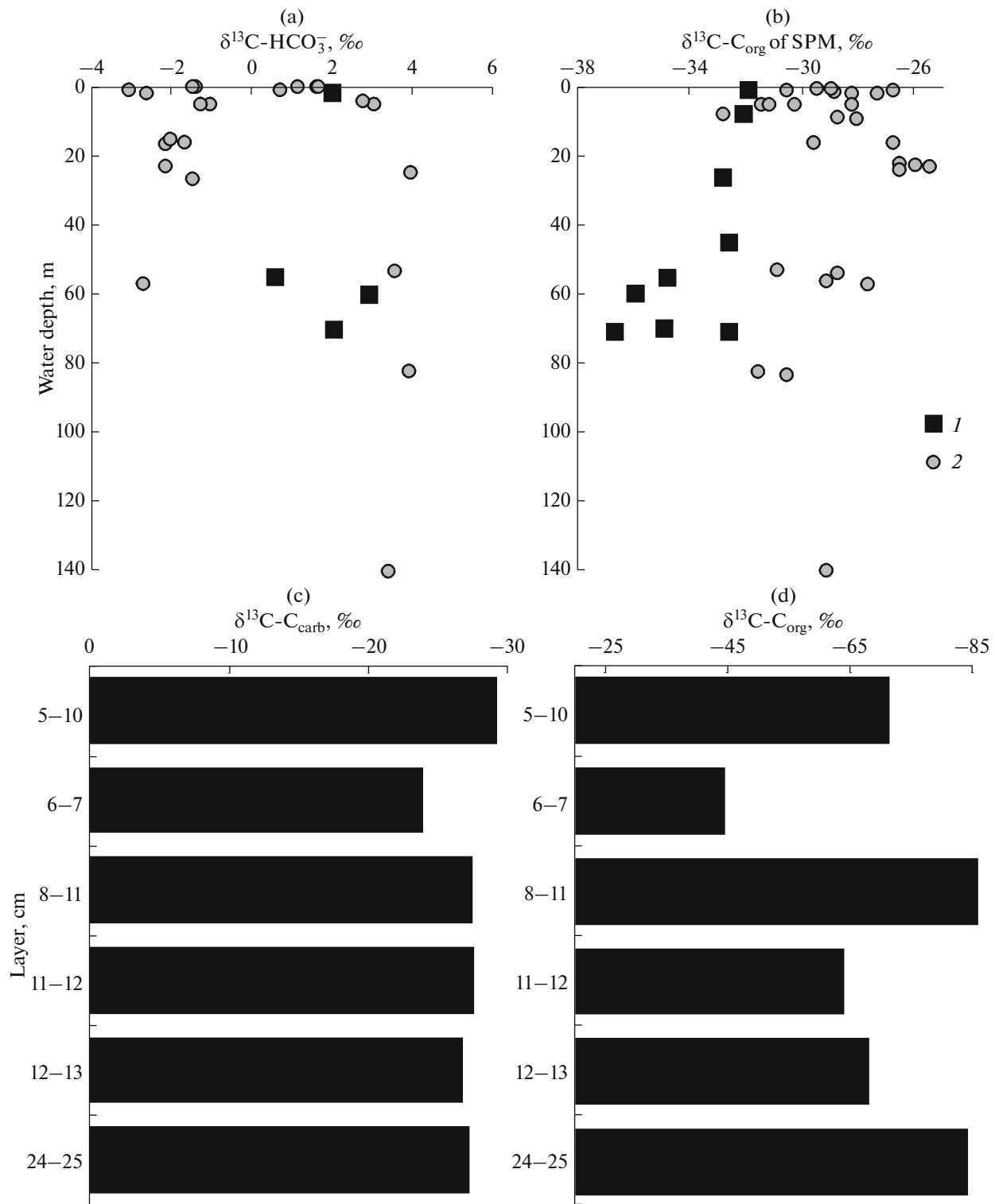


Fig. 3. Carbon isotope values $\delta^{13}\text{C-HCO}_3^-$ of water (a), $\delta^{13}\text{C-C}_{\text{org}}$ of SPM (b) and $\delta^{13}\text{C-C}_{\text{carb}}$ (c) and $\delta^{13}\text{C-C}_{\text{org}}$ of carbonate concretions (d) of the Laptev Sea shelf. 1—Samples collected at methane seep site; 2—background samples.

ering, a strong hydrogen sulfide odor, and high methane concentrations. They were assigned a Holocene age. Sediment water content varied from 58% at the top to 32% at the bottom of the 49-cm long sediment core.

Some of the Neymiste tube samples have a thin, up to 1–2 cm wide oxidized layer on their surface.

Box core samples were recovered from the sedimentary interval with high densities of siboglinid

Table 2. Chemical composition of carbonate concretions and host sediments at seep site, %

Nos.	Sampling tool	Layer, cm	LOI %	SiO ₂	Al ₂ O ₃	TiO ₂	Fe	MnO	K ₂ O	CaO	MgO	Na ₂ O	P ₂ O ₅	Sr	Ba	Zr	Cr	S
Carbonate concretions																		
1	NT-2	5-10	23.62	33.80	6.55	0.38	1.92	0.13	1.53	26.15	2.81	1.47	0.17	0.229	0.035	0.012	0.007	0.357
2	GC-2	8-11	27.58	26.51	5.01	0.36	1.61	0.31	1.22	31.50	2.80	1.38	0.34	0.187	0.028	0.014	0.006	0.271
3	GC-2	11-12	28.55	25.65	5.07	0.31	1.61	0.28	1.15	31.66	2.93	1.33	0.31	0.186	0.031	0.014	0.006	0.186
4	GC-2	12-13	27.99	27.02	5.07	0.30	1.52	0.26	1.19	30.87	2.73	1.58	0.30	0.185	0.034	0.014	0.007	0.254
Host sediments																		
1	NT-1	1-3	7.07	59.69	15.59	0.66	4.66	0.03	2.77	1.27	2.11	3.42	0.16	0.022	0.052	0.020	0.006	0.682
2	NT-1	3-15	7.7	58.25	14.32	0.60	4.10	0.06	2.75	4.69	2.12	3.1	0.17	0.035	0.054	0.024	0.005	0.462
3	NT-2	8-15	4.66	65.67	13.98	0.59	3.47	0.07	2.82	1.63	1.68	3.0	0.12	0.029	0.065	0.028	0.004	0.931
4	GC-1	10-15	5.87	61.76	14.49	0.62	3.65	0.04	2.8	3.68	2.0	3.14	0.17	0.034	0.062	0.024	0.011	0.291
5	GC-1	36-44	6.7	60.91	13.84	0.64	3.59	0.06	2.68	4.5	2.0	3.02	0.19	0.036	0.058	0.036	0.007	0.392
6	GC-1	41-49	4.02	66.23	13.73	0.70	3.61	0.05	2.78	1.92	1.72	3.12	0.14	0.031	0.068	0.053	0.006	0.520
7	GC-2	4-9	4.87	63.56	14.33	0.65	3.69	0.07	2.83	2.95	1.85	3.15	0.13	0.032	0.060	0.034	0.004	0.441
8	GC-2	16-28	4.41	65.74	13.11	0.67	3.26	0.06	2.77	3.36	1.64	2.92	0.13	0.035	0.060	0.049	0.005	0.612

pogonophorans, which is hereinafter referred to as pogonophoran field.

Repeated sampling did not penetrate below a depth of 49 cm (GC-1), probably due to the compact sediment. Deeper penetration of a gravity corer was prevented by the presence of carbonate concretions forming within layers of sedimentary strata and probably by the underlying layer of relict permafrost [12].

The bulk chemical composition of both host and background sediments within the cold seep site (st. 5231) is dominated SiO₂ (58–66% dry weight), Al₂O₃ (14–16%) and Fe (3.5–4.6%) (Table 2).

The concentrations of CaO (1.27–4.6%) and Sr, Ba, Zr, Cr, and S were much higher in host muds than in background sediments (Table 2).

Higher concentrations of Fe and S in host sediments can be explained by the presence of hydrotroilite, pyrite, etc., derived from hydrogen sulfide. The main mineralogy of sediments from the methane seep and background sediments was found to be similar and includes quartz and feldspar.

The C_{org} content of host sediments varied from 0.38 to 0.5% between 5–10 and 24–25 cm depth (Table 3), reaching 1.9% in the upper silt (0.0–0.5 cm) layer.

The concentration of dissolved organic carbon (DOC) in sediments reached 149 mg/L (2–7 cm layer) at stations closest to the seep (st. 5224), which was two to three times higher than that of background sediments collected far from the seep (Table 4).

The methane concentration in sediments from the seep site varied from 200–300 μL/L in the upper 10 cm to 10462 μL/L at 44 cm (GC-2) (Table 5). The highest CH₄ concentration (12064 μL/L) was detected within

the pogonophoran field, in a sample taken with a make-shift bulb syringe. This value is 5–6 orders of magnitude higher than the methane concentrations in the surface sediment layers at background shelf stations.

The above results, including the high concentrations of free hydrogen sulfide (>0.04 mg/L) and methane, as well as elevated concentrations of DOC, C_{org}, Fe, and S in recent sediments, are indicative of a reducing environment in sediments hosting carbonate concretions. This is supported by the results of radioisotope tracer experiments on the rates of anaerobic microbial processes (Table 5).

The isotopic composition of C_{org} and C_{carb} in background sediments (stations in the across-shelf transect) reflects the contribution of terrigenous OM and riverine carbonate, respectively, to the composition of sedimentary–diagenetic dispersed carbonate at station 5225 located farthest from the Lena River delta (Table 3).

Carbonate concretions. Carbonate concretions of variable size (up to ~5 cm) and morphology are most abundant (50–60%) in core GC-1 at 17–27 cm but decrease downcore at 27–30 cm (Fig. 5). They are more abundant (up to 89%) in core GC-2 at 8–10 cm in black fine silt mud. In the lower 10–23 cm layer, all carbonate concretions are found in the upper fine silt layer and at the base of the coarse silt layer.

In samples collected with Neymiste tubes (NT-1 and NT-3), carbonate concretions (up to 0.5 cm in size) are found at the base of the 0.5–13 cm layer of intensely bioturbated black semiliquid and soft mud, which becomes more compact with depth.

Thus, the carbonate concretions are found across the entire cored interval of recent sediments within the

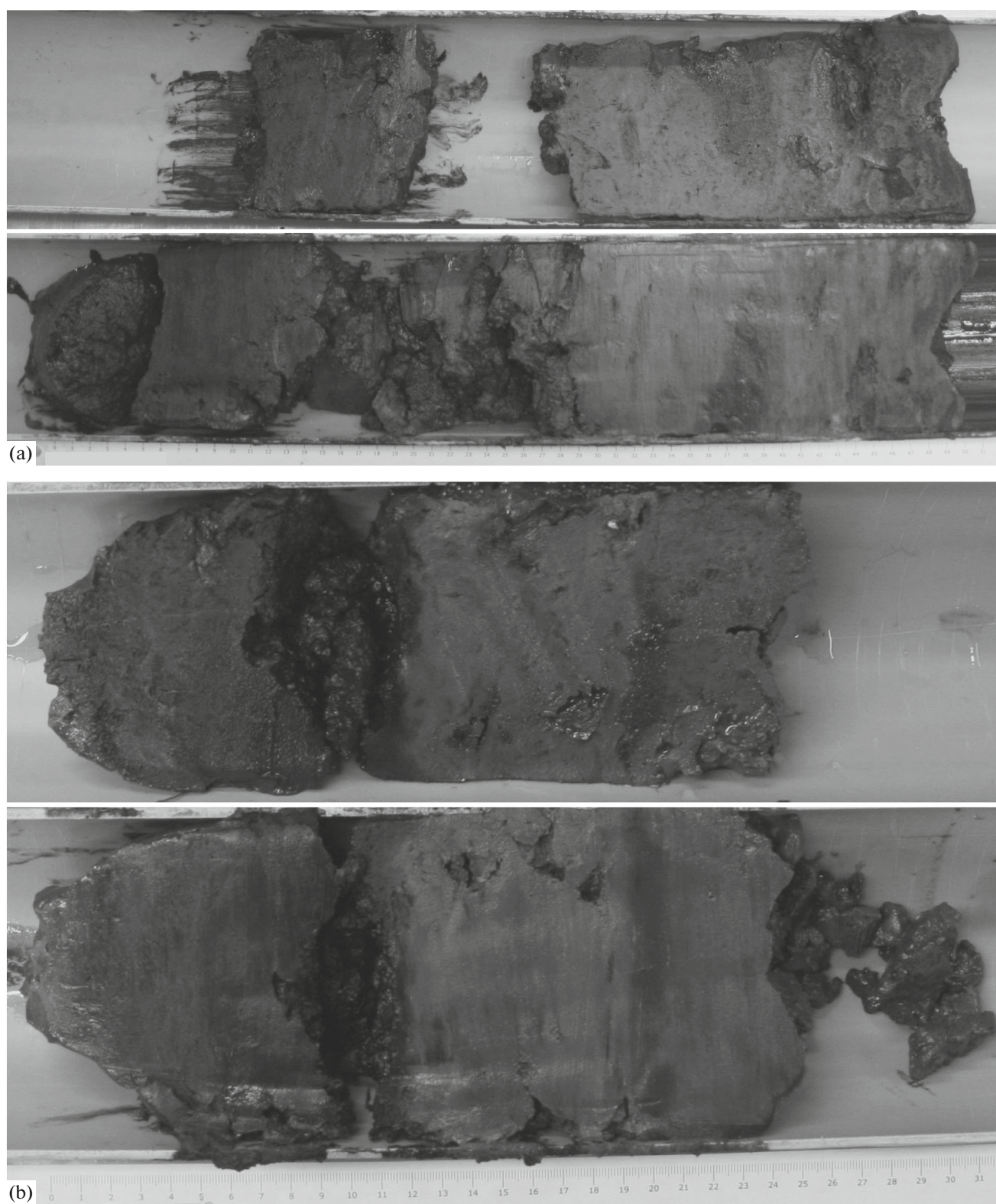


Fig. 4. Photographs of bottom sediment cores with natural water content and intercalations of carbonate concretions collected using a GC tool at cold methane seep site: (a) GC-1, 0–49 cm; (b) GC-2, 0–23 cm. Photos courtesy of A.I. Mamochkina.

Table 3. Content and isotopic composition of C_{org} and C_{carb} in carbonate concretions and host sediments at seep site and in bottom sediments at background stations (n.d., not determined)

Station Depth, m	Layer, cm	Sampling tool	C_{carb}	C_{org}	$\delta^{13}C-C_{carb}$	$\delta^{13}C-C_{org}$	Carbonate minerals
			%		‰		
Carbonate concretions							
Site	5–10	NT-2	6.74	0.499	–29.14	–71.13	Mg-calcite, aragonite
71	6–7	GC-2	3.45	0.24	–23.83	–44.47	Mg-calcite
	8–11	GC-2	7.65	0.55	–27.36	–88.47	Mg-calcite
	11–12	GC-2	8.08	0.475	–27.51	–63.82	Mg-calcite
	12–13	GC-2	8.31	0.472	–26.66	–67.90	Mg-calcite
	24–25	GC-1	5.00	0.76	–27.16	–83.95	Mg-calcite
Host sediments							
Site	0–0.5	NT-1	0.19	1.89	tr	–28.48	No carbonates
71	1–3	NT-1	0.17	1.06	–2.78	–31.31	No carbonates
	3–15	NT-1	0.67	1.12	–13.42	–29.50	No carbonates
	8–15	NT-2	0.32	0.46	–12.09	–32.88	No carbonates
	10–15	GC-1	0.99	0.53	–14.44	–30.80	No carbonates
	20–21	GC-1	1.10	0.73	–	–	No carbonates
	36–41	GC-1	1.20	0.52	–12.04	–32.15	No carbonates
	41–49	GC-1	0.42	0.41	–6.83	–27.66	No carbonates
	4–9	GC-2	0.57	0.47	–12.14	–35.70	No carbonates
	16–23	GC-2	0.71	0.38	–13.39	–36.08	No carbonates
Background sediments							
st. 5223	0–2	NT	0.27	1.15	n.d.	–27.47	No carbonates
56	2–12	NT	0.23	0.88	n.d.	–27.03	No carbonates
	12–19	NT	0.22	0.69	n.d.	–25.98	No carbonates
st. 5224	0–2	NT	0.21	0.52	n.d.	–25.47	No carbonates
57	2–7	NT	0.18	0.71	n.d.	–25.96	No carbonates
	7–18	NT	0.14	0.43	n.d.	–28.63	No carbonates
st. 5228	0–2	NT	0.12	0.42	n.d.	–27.55	No carbonates
87.2	2–8	NT	0.11	0.58	n.d.	–	No carbonates
	8–13	NT	0.14	0.81	n.d.	–	No carbonates
st. 5229	10–20	GC	0.27	0.90	n.d.	–	No carbonates
87	50–60	GC	0.29	0.98	n.d.	–	No carbonates
	100–110	GC	0.22	0.99	n.d.	–26.41	No carbonates
st. 5227	0–2	Grab	n.d.	n.d.	–18.20	–26.70	No carbonates
1979							
st. 5225	0–2	Grab	n.d.	n.d.	–14.90	–27.70	No carbonates
2385	9–11	Grab	n.d.	n.d.	–16.30	–27.80	No carbonates
	11–17	Grab	n.d.	n.d.	–22.80	–27.60	No carbonates

methane seep site: between 5–10 cm (NT-2) and 27–30 cm (GC-1) (Table 3). Concretions are colored black with sticky mud or can be washed clean (with distilled water at pH adjusted to their native habitats). Carbonate concretions appear rather uniform in their morphologies (Fig. 5). They usually range from poorly consolidated to well consolidated flat crusts or have a dumbbell and dendritic habit, with numerous small-diameter (~1 mm) or locally large-diameter (~1–3 mm) canals and large caverns. These concretions range in size from 1 to 5 cm and may resemble in their morphologically and size the carbonate

concretionary structures of the Kara Sea from a water depth of 55 m (st. 5032, Fig. 1a) [9].

Most of the studied carbonate concretions exhibit a highly bioturbated and, rarely, zoned microstructure manifested along and around burrows of mud-eaters. Burrows are filled with terrigenous clasts of different minerals with pelitomorphic clay–carbonate cements. Mg-calcite with clay minerals and minor amounts of detrital grains deposited along the external surfaces of burrow walls. Pores in the newly formed concretions are frequently open or may be filled with late Mg-cal-

cite or similar crystals of Mg-calcite and aragonite in the 5–10 cm layer.

Thin section examination indicates that the internal structure of carbonate concretions is comprised of detrital grains varying in their size range (from 0.01 to 0.10 mm), composition, and roundness (from angular to subrounded), with carbonate, carbonate-clay and, more rarely, clay-carbonate cements (Fig. 6). Several types of cement are identified, such as the principal pore-lining carbonate cement between detrital grains, pore-filling carbonate-clay and pelitomorph clay-carbonate cements.

Detrital grains enclosed in cement include quartz, plagioclase, feldspar, amphibole, etc., with accessory (<1%) actinolite, pyroxene, epidote, zircon, muscovite, biotite, garnet, sphene, and ore minerals. Clay minerals in the cement are mostly illite, and minor kaolinite, chlorite, and smectite (Table 6).

In all carbonate concretions, the cement is Mg-calcite, while aragonite cement is known only in the youngest sediments collected at 5–10 cm (NT-2) and 6–7 cm (GC-2) (Fig. 7).

Microstructural studies and spectral analysis reveal the following polymorphs of authigenic carbonate minerals (Fig. 7):

(1) Isomorphic calcium carbonate (CaCO₃) with the invariant presence of Mg (~2%). This structural variety of Mg-calcite (average ~30 μm) cements both detrital and clay minerals and occurs as a pore-lining and, more rarely, pelitomorph pore-filling cement. Scalenohedral calcite crystals form columnar intergrowths and penetration twins at contact with mineral grains. The crystallinity of Mg-calcite increases upward from the base of the sampled interval.

(2) Phanerocrystalline Mg-calcite (containing ~3% Mg) forming scalenohedral crystals (average ~30 μm). Crystal druses fill pores and cavities in the carbonate concretions. This Mg-calcite variety was not found at the base of the sampled interval.

(3) Phanerocrystalline Mg-calcite (containing ~3% Mg) forming rhombohedral crystals (average ~20 μm). These crystals often occur as aggregates after scalenohedral Mg-calcite crystals filling pores and appear to be a late generation of Mg-calcite. This Mg-calcite variety was not found at the base of the sampled interval.

(4) Large (up to ~170 μm) prismatic aragonite (a polymorphic phase of calcite) crystals, often forming twins or triplets, as well as aggregates represented by radially fibrous or parallel-columnar intergrowths of crystals. Aragonite contains up to ~1% Sr. Unlike the Mg-calcite cement and secondary phanerocrystalline Mg-calcite, aragonite occurs as long-prismatic crystals inside cement pores or may line the pores, together with scalenohedral Mg-calcite crystals, in pelitomorph clay-carbonate cement (Fig. 7).

Table 4. DOC concentrations in pore water at background stations

Station Depth, m	Layer, cm	DOC, mg/L	Note
st. 5225 2385	2–9 9–11	19.99 15.75	At a distance from the seep site
st. 5224 57	0–2 2–7 7–18	15.17 149.16 57.12	Closest to the seep site
st. 5215/2 26	0–2 3–10 10–22	39.85 48.66 46.65	Near the Lena River delta

Data provided by N.V. Lobus, Shirshov Institute of Oceanology, Russian Academy of Sciences.

The crystallization of pyrite in paragenesis with Mg-calcite took place with the involvement of microorganisms (Fig. 7). Pyrite is the major form of iron disulfide in the carbonate concretions and occurs as isolated spherical grains (~1 μm) or framboids (up to 6.4 μm).

Some carbonate concretions may contain abundant organic debris (fragments of floral and faunal remains) overgrown by iron hydroxides forming mats and chains (GC-2, 8–11 cm). The presence of organomineral films was detected locally in some concretions.

Finely disseminated organic matter and very fine coal attritus are present as inclusions in thin sections (Fig. 6). The C_{org} content of carbonate concretions was less than 1% (Table 3).

The δ¹³C-C_{carb} value of authigenic Mg-calcite from carbonate concretions varied from –24 to –23‰ in different sedimentary layers (Table 3, Fig. 3c). This isotopic composition suggests that Mg-calcite was produced during diagenesis by the microbial degradation of isotopically light organic matter in the host sediments with the involvement of carbon dioxide formed via oxidation of methane. This is also seen from δ¹³C-C_{org} values of carbonate concretions with an anomalously light isotopic composition (from –44.5 to –88.5‰) (Table 3, Fig. 3d).

DISCUSSION

The Arctic shelf seas are unfavorable for carbonate precipitation. The same is true for recent sediments of the Laptev Sea. Nevertheless, these sediments, similar to those of the White Sea, Kara Sea, and other Arctic seas, are characterized by the presence of hard diagenetic carbonate concretions composed of terrigenous detrital material with Mg-calcite (up to 40%) and clay cements [2, 3, 10].

Marine sediments at the seep site hosting such diagenetic carbonate buildups were deposited on the continental shelf deeply incised by paleovalleys [25],

Table 5. CH₄ concentration and rates of microbial processes in bottom sediments at the seep site and background stations. Abbreviations: MO, methane oxidation; DAC, dark CO₂ assimilation

Station depth, m	Sampling tool	Layer, cm	CH ₄ , μL L ⁻¹	MO, nMCH ₄ dm ⁻³ d ⁻¹	DAC		
					μgC dm ⁻³ d ⁻¹	μMC dm ⁻³ d ⁻¹	
Site 71	NT-1	0–1	430	104	87	7.25	
		2–4	732	966	34	2.83	
		8–10	n.d.	431	31	2.58	
		14–16	n.d.	394	25	2.08	
	NT-2	8–12	1151	495	n.d.	n.d.	
	NT-3	5–11	n.d.	647	41	3.42	
	NT-4	6–12	n.d.	275	n.d.	n.d.	
	GC-1	4–5	283	163	31	2.58	
		10–11	223	538	25	2.08	
		37–38	8622	315	11	0.92	
		44–45	10462	432	22	1.83	
		Pogonophoran field					
	BC	0–4	12064	3040	485	40.42	
Microbial mats							
“Bulb syringe”	0–1	5178	515	137	11.42		
st. 5225	Grab	0–2	0.43	n.d.	–	–	
2385		9–11	0.51	n.d.	–	–	
		11–17	0.56	n.d.	–	–	
st. 5228	NT	0–2	1.04	n.d.	–	–	
87.2		14–16	0.74	n.d.	–	–	
st. 5229	GC	10–11	0.53	n.d.	–	–	
87		72–73	0.85	n.d.	–	–	
		122–123	0.64	n.d.	–	–	
		222–223	1.07	n.d.	–	–	
st. 5224	NT	0–2	0.75	n.d.	–	–	
57		15–17	0.92	n.d.	–	–	
st. 5223	NT	0–2	0.85	n.d.	–	–	
56		16–18	0.95	n.d.	–	–	
st. 5215-2	NT	0–2	1.19	n.d.	–	–	
26		15–17	0.95	n.d.	–	–	
st. 5218	NT	0–3	1.87	n.d.	–	–	
18		5–8	1.51	n.d.	–	–	
		22–25	1.69	n.d.	–	–	
Kara Sea shelf, after [13]							
st. 4960	NT	0–1	0.67	1.0	22.8	1.9	
120		1–7	1.59	200	86.2	7.2	
st. 4990	GC	0–1	1.04	181	98.2	8.2	
114		1–7	1.53	234	113	9.4	
		7–15	1.33	190	118	9.8	
		90–100	2.82	167	134	11.2	

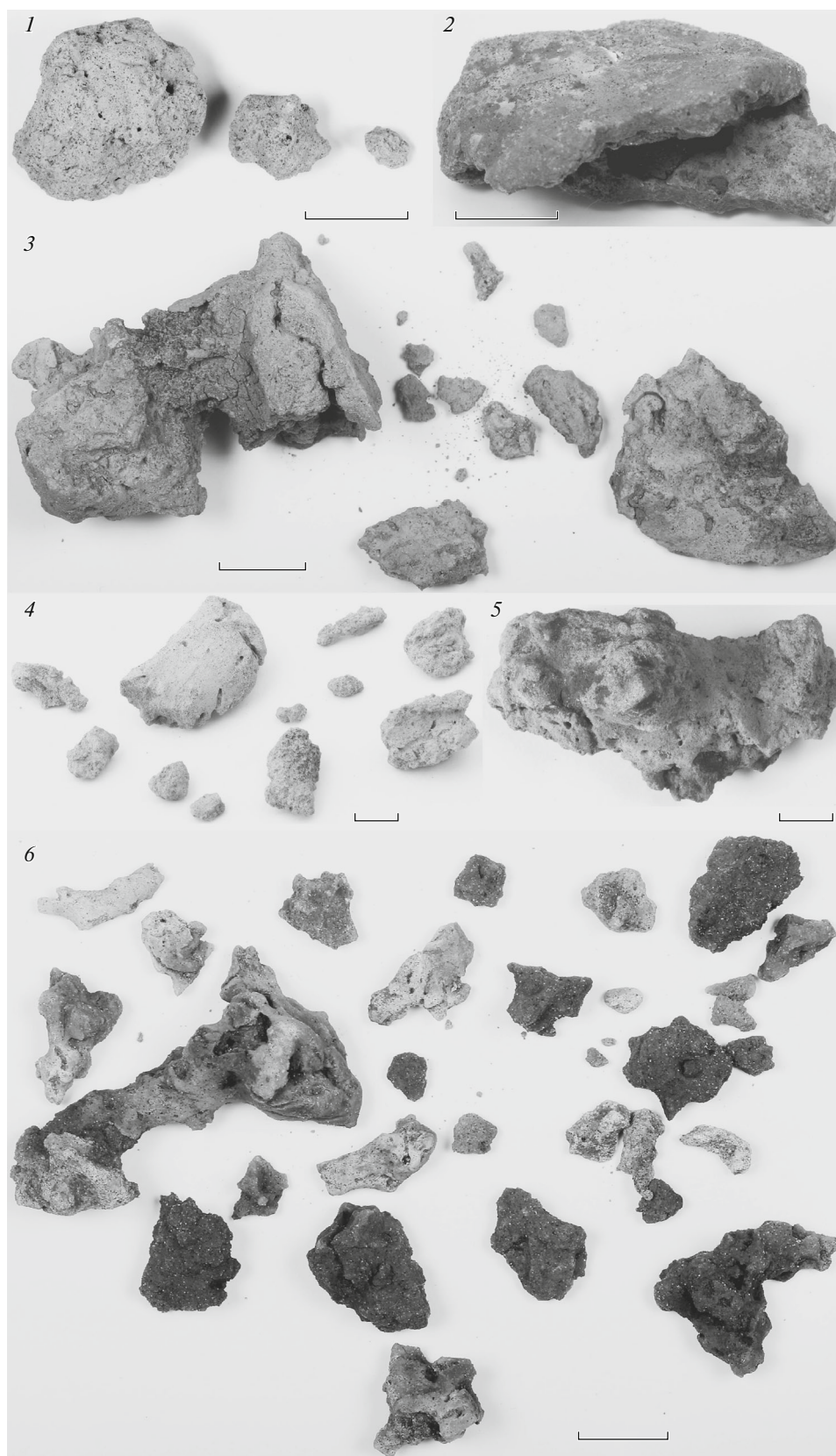


Fig. 5. Photographs of carbonate concretions recovered from different intervals of bottom sediments at methane seep site, Laptev Sea: 1—GC-1, 24–25 cm sediment layer; 2—GC-2, 6–7 cm; 3—GC-2, 8–11 cm; 4—GC-2, 11–12 cm; 5—GC-2, 12–13 cm; 6—NT-2, 5–10 cm; 7—pores and caverns on surface of concretions and concretion interiors (cut). Scale in photo is 1 cm. Photos courtesy of film studio of Shirshov Institute of Oceanology, Russian Academy of Sciences.

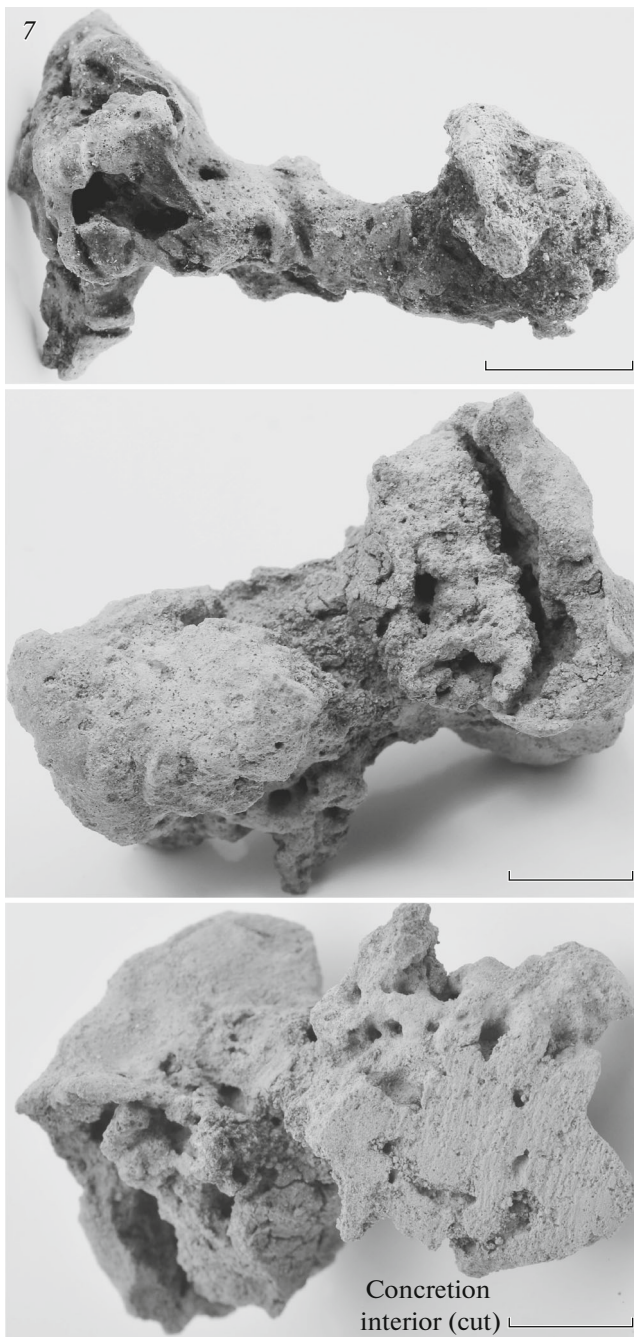


Fig. 5. (Contd.)

which was once subaerially exposed before marine transgression.

Avalanche sedimentation of riverine suspended sediments under conditions of high salinity gradients that occurred in paleovalleys as a consequence of rapid sea-level rise during Holocene marine transgressions and shoreface retreat [20].

As a result, the paleovalley fill is represented by poorly sorted terrigenous, silt-sized, sediments, exhibiting a high degree of bioturbation.

Grain size, roundness, and composition of terrigenous clasts indicate repeated redeposition and long-distance transport from their continental sources.

The carbonate concretions from the seep site were formed during early diagenesis of terrigenous–clays marine sediments of the Arctic seas deposited as a result of multiple marine transgression–regression cycles during the Holocene [4]. These marine deposits are underlain by a thick layer of relict permafrost. Romanovsky and Hubberten [12] showed that on the Arctic shelf of East Siberia, the accumulation of gas below the permafrost took place in periods of marine regression, while the emission of gas on the outer shelf through permafrost thaw ponds and discontinuities in the gas hydrate stability zone occurs in periods of marine transgression.

Carbonate concretions within sedimentary layers are usually concentrated at the lithological boundary, i.e., at possible gas migration paths.

At the seep site, hydrogen sulfide and methane were detected in near-bottom water and sediment layers. The reducing Eh values (from -100 to -120 mV) and alkaline pH (>7.5) indicate conditions favoring the precipitation of carbonates from early colloidal material and the formation of variably crystalline carbonate cement.

The carbonate concretions of broadly similar types are found at several intervals within the sampled sedimentary sequence. They are characterized by the presence of burrows, bioturbation, and inequigranular textures. This carbonate buildup is formed by aggregates of detrital grains that line or fill burrows and by pelitomorphic clay–carbonate cements around burrows.

Carbonate concretions and their host sediments are characterized by the presence of similar detrital and clay minerals. Mineralogical variability can be explained by a wide range of sediment transport to the Arctic shelf seas, including transport by rivers, sea ice, and ice exaration.

Carbonate minerals in these concretions are represented at least by three generations (structural varieties) of Mg-calcite. In addition to Mg-calcite, well-developed prismatic aragonite crystals and aggregates were detected in carbonates from the uppermost (5–10 cm) layer. Aragonite is likely to have formed by dissolution and redeposition of shelly detritus. The presence of aragonite led to an increase in Sr (0.23%) and a decrease in MnO (0.13%) in the concretions recovered at 5–10 cm, as compared to the concretions with higher carbonate contents from the lowermost layers of the sampled interval (Table 2).

The most likely source of carbonate carbon in concretions was oxidation of carbon in organic matter from the host sediments via sulfate reduction. Thus, the carbon in carbon dioxide that is formed by sulfate reduction inherits the isotopic composition of the sedimentary C_{org} ($\delta^{13}C-C_{org} = -27\text{‰}$), which is typical of allochthonous organic matter in the study area (Table 3).

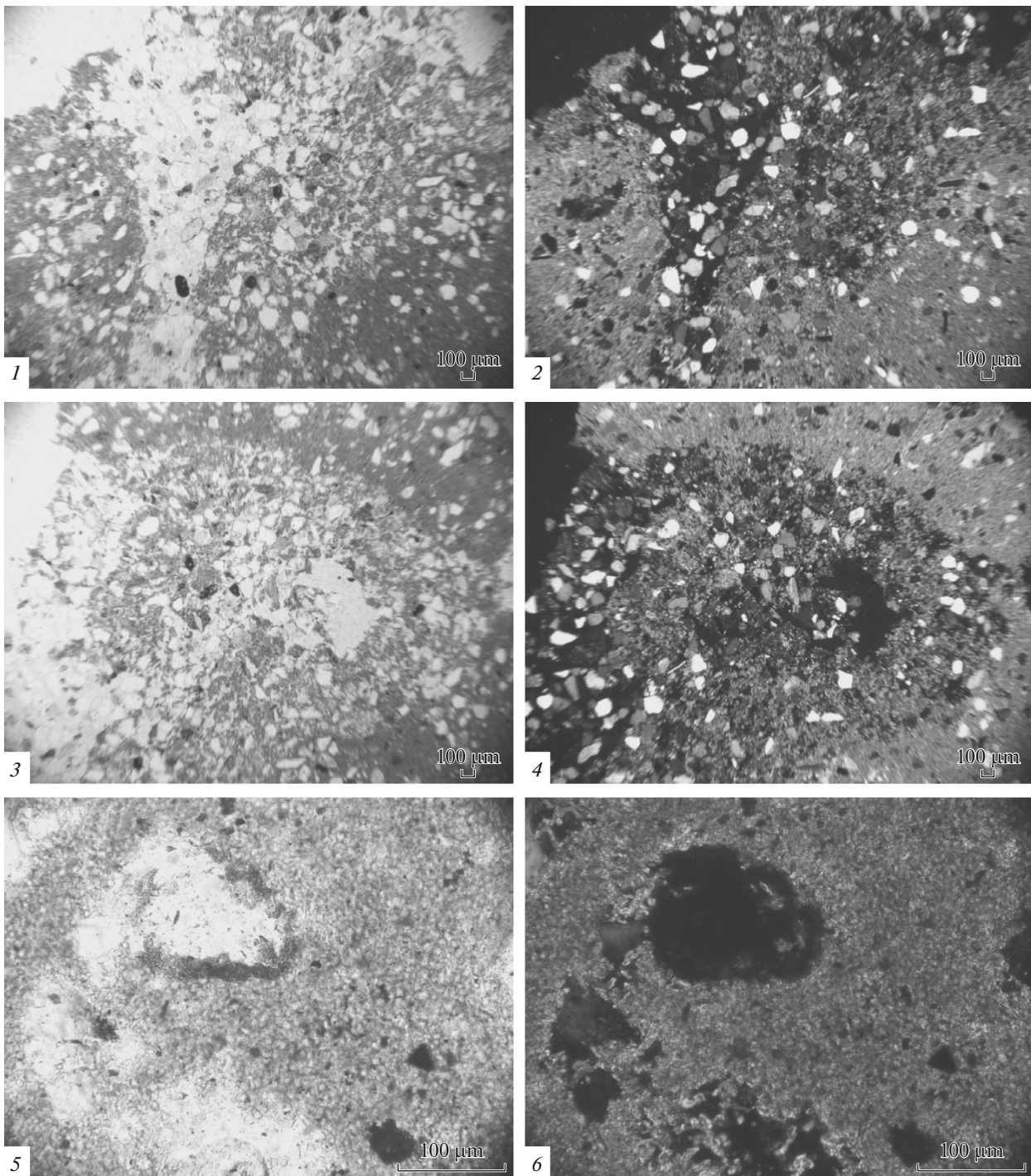
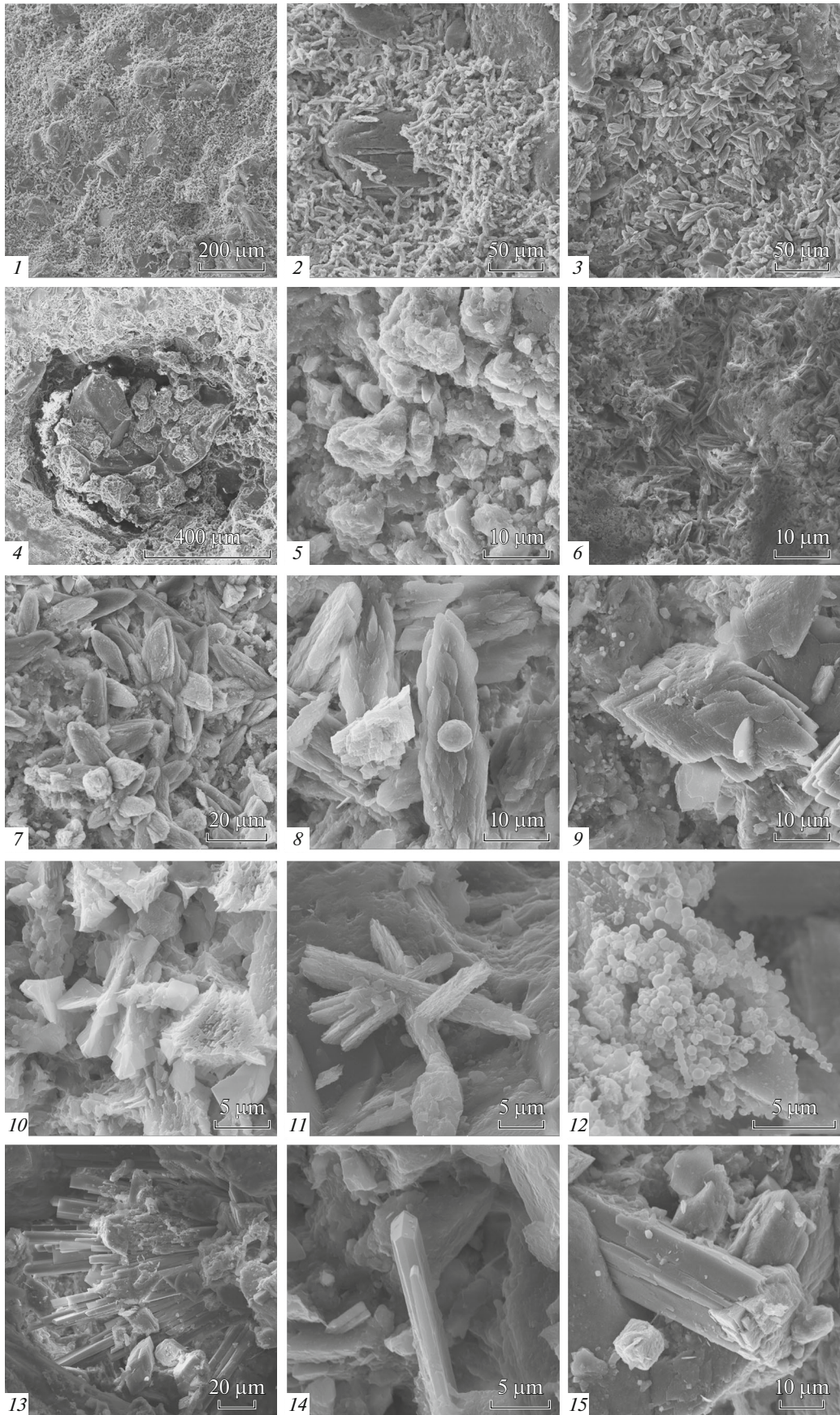


Fig. 6. Photomicrographs of thin sections of carbonate concretions, methane seep site: 1, 2—sign of bioturbation, vertical section of burrow (1—parallel nicols, 2—crossed nicols); 3, 4—sign of bioturbation, cross section of burrow (3—parallel nicols, 4—crossed nicols); 5, 6—pores filled with organic matter (5—parallel nicols, 6—crossed nicols). Scale in upper right-hand corner of image is 100 µm.

Fig. 7. Photomicrographs of fresh chips of carbonate concretions, methane seep site: 1, 2—Mg-calcite cement, detrital minerals of quartz-feldspar composition (GC-2, 6–7 cm); 3—Mg-calcite cement filling pore space of concretions, well crystallized grains of Mg-calcite (GC-2, 8–11 cm); 4—pore filled with detrital quartz grains and clay; 5—clay-carbonate material filling a pore (NT-2, 5–10 cm); 6—carbonate-clay material filling a pore (PC-2, 11–12 cm); 7—scaleno-hedral Mg-calcite crystals (PC-2, 8–11 cm); 8—two generations of Mg-calcite grains and pyrite framboid (PC-2, 12–13 cm); 9—rhombohedral Mg-calcite crystals, individual spherical pyrite grains (NT-2, 5–10 cm); 10—intergrowth of Mg-calcite grains, two polymorphs of Mg-calcite (PC-2, 6–7 cm); 11—intergrowth of poorly crystallized calcite grains (GC-1, 24–25 cm); 12—iron hydroxides developed after Mg-calcite crystals (GC-2, 8–11 cm); 13—radially fibrous aggregate of Sr-aragonite, rhombohedral Mg-calcite crystals in a pore; 14—prismatic crystal of Sr-aragonite; 15—intergrowth of Sr-aragonite and Mg-calcite crystals (NT-2, 5–10 cm).



Early diagenetic processes in the seep site were affected by seepage of isotopically light methane ($\delta^{13}\text{C}\text{-CH}_4 \sim 70\%$) through the sediment hosting carbonate concretions. Anaerobic oxidation of methane at a rate of $104\text{--}515 \text{ nM dm}^{-3} \text{ d}^{-1}$ (and up to $3040 \text{ nM dm}^{-3} \text{ d}^{-1}$ in the pogonophoran field) resulted in the release of additional fluxes of carbon dioxide, which was involved in the dissolution and recrystallization of an early colloidal and late Mg-calcite cement (Table 5). This resulted in the formation of well-developed scalenohedral and rhombohedral crystals, the second and third polymorphic forms of Mg-calcite.

In summary, it should be emphasized that the presence of three generations of Mg-calcite (aragonite) can be explained by superimposition of carbonate formation via methane oxidation onto the early-stage authigenic carbonates in areas with high sedimentary C_{org} contents, i.e., in sediments inhabited by benthic invertebrates. These organisms promote the redistribution of the most mobile components of organic matter and minerals from the water–seafloor boundary up to sediment depths of ~ 40 cm. The degradation of this organic matter and the production of CO_2 result in the precipitation of carbonate minerals around burrows (e.g., pogonophorans). The subsequent influx of methane-bearing fluids to the sediment and anaerobic oxidation of methane provide an additional source for recrystallization and precipitation of phanerocrystalline Mg-calcite varieties and coarsely crystalline aragonite filling the pore spaces in a pelitomorphous clay–carbonate cement.

The involvement of anaerobic oxidation of methane in the precipitation of carbonate concretions is confirmed by the light isotopic composition of C_{org} , ranging between -44.5 and -88.5% (Table 3). The anomalously low $\delta^{13}\text{C}\text{-}C_{\text{org}}$ values of carbonate concretions are indicative of very slow rates of microbial methane oxidation.

Isotope mass balance calculations show that the carbonate concretions contain up to $65\text{--}83\%$ sedimentary–diagenetic Mg-calcite and $17\text{--}35\%$ methane-derived Mg-calcite.

It should be noted that no ikaite was found in recent sediments at methane seep site, which was characterized by favorable conditions for its precipitation: low water temperatures at the bottom and methane fluxes.

CONCLUSIONS

This study provides the first evidence for large, hard carbonate concretions in recent marine sediments of the Laptev Sea shelf. These carbonates are interpreted to have been derived from carbon dioxide produced via degradation of sedimentary organic matter, bacterial sulfate reduction and anaerobic microbial oxidation of methane. It was shown that the stud-

ied concretions differ in their morphology, textural and structural features from carbonate concretions previously described in bottom sediments of the Arctic seas (Figs. 1, 5) [2–5, 7, 9, 17–19, 21–24].

The isotopic composition of carbonate and organic carbon in authigenic carbonate concretions provide information on the genesis of carbon dioxide, as well as sedimentary and concretionary C_{org} .

Authigenic carbonate formation in the Arctic shelf seas can act as a biogeochemical filter mechanism limiting methane emissions from bottom sediments to the water column and atmosphere.

ACKNOWLEDGMENTS

The authors are grateful to Academicians A.P. Lisitzin and M.V. Ivanov for supporting this study; A. Yu. Miroshnikov for his assistance with sample selection and preparation of thin sections; A.N. Novigatsky, A.I. Mamochkina, V.V. Markelov, G.V. Malafeev, A.A. Udalov, V.Yu. Rusakov, and Z.Yu. Redzhepova for their help with sediment sampling; S.A. Shchuka for providing hydrophysical data; and A.G. Boev, T.S. Prusakova, I.I. Rusanov, N.V. Lobus, and A.A. Polukhin for their assistance with sample analyses.

Expedition studies were carried out with the support of the Russian Foundation for Basic Research (project no. 14-05-05003Kar_a). Laboratory researches were supported by the Presidium of the Russian Academy of Sciences (project no. I.32P). The study of carbon isotopic composition of methane, organic matter, and carbonates was supported by the Russian Foundation for Basic Research (project no. 14-04-00682). The results were interpreted as part of a state assignment of the Shirshov Institute of Oceanology, Russian Academy of Sciences, for 2015–2017 (project no. 0149–2014–0026) and Russian Science Foundation (project no. 14-17-00681).

REFERENCES

1. P. L. Bezrukov and A. P. Lisitzin, "Classification of sediments of modern marine reservoirs," *Tr. Inst. Okeanol., Akad. Nauk SSSR* **32**, 3–14 (1960).
2. E. M. Galimov, L. A. Kodina, O. V. Stepanets, and G. S. Korobeinik, "Biogeochemistry of the Russian Arctic. Kara Sea: research results under the SIRRO project, 1995–2003," *Geochem. Int.* **44**, 1053–1104 (2006).
3. A. R. Geptner, V. V. Petrova, and O. S. Vetoshkina, "New data on the composition of stable isotopes in glendonites of the White Sea and their genesis," *Lithol. Miner. Res.* **49**, 473–490 (2014).
4. E. A. Gusev, A. P. Matyushev, A. S. Rudoi, and A. N. Usov, "Quaternary sediments of the central part of Kara Sea," in *The Results of System Oceanological Studies in Arctic*, Ed. by A. P. Lisitzin (Nauchnyi Mir, Moscow, 2001), pp. 553–558.

5. M. E. Kaplan, "Calcite pseudomorphs (pseudogeimocent, gerovit, thinolite, glendonite, White Sea flyers) in sedimentary minerals. Origin of pseudomorphs," *Litol. Polezn. Iskop.*, No. 5, 125–141 (1979).
6. A. A. Krylov, E. A. Logvina, T. V. Matveeva, et al., "Ikait ($\text{CaCO}_3 \cdot 6\text{H}_2\text{O}$) in bottom sediments of the Laptev Sea and role of anaerobic oxidation of methane during its formation," *Zap. Ross. Mineral. O-va* **144** (4), 61–75 (2015).
7. A. Yu. Lein, "Authigenic carbonate formation in the ocean," *Lithol. Miner. Resour.* **39**, 1–30 (2004).
8. A. Yu. Lein and M. V. Ivanov, *Biogeochemical Cycle of Methane in the Ocean* (Nauka, Moscow, 2009) [in Russian].
9. A. Yu. Lein, P. N. Makkaveev, A. S. Savvichev, M. D. Kravchishina, N. A. Belyaev, O. M. Dara, M. S. Ponyaev, E. E. Zakharova, A. G. Rozanov, M. V. Ivanov, and M. V. Flint, "Transformation of suspended particulate matter into sediment in the Kara Sea in September of 2011," *Oceanology* (Engl. Transl.) **53**, 570–606 (2013).
10. A. Yu. Lein, I. I. Rusanov, N. V. Pimenov, A. S. Savvichev, Yu. M. Miller, G. A. Pavlova, and M. V. Ivanov, "Biogeochemical processes of the sulfur and carbon cycles in the Kara Sea," *Geochem. Int.* **34**, 925–941 (1996).
11. A. P. Lisitzin and V. P. Petelin, "The method of preliminary processing of samples of marine sediments aboard a vessel," *Tr. Inst. Okeanol., Akad. Nauk SSSR* **19**, 240–251 (1956).
12. N. N. Romanovskii and H.-W. Hubberten, "The permafrost zone and zone of stability of gas hydrates on the shelf of Laptev Sea: the decade Russian–German research results," *Kriosfera Zemli* **10** (3), 61–68 (2006).
13. A. S. Savvichev, E. E. Zakharova, E. F. Veslopolova, I. I. Rusanov, A. Yu. Lein, and M. V. Ivanov, "Microbial processes of the carbon and sulfur cycles in the Kara Sea," *Oceanology* (Engl. Transl.) **50**, 893–908 (2010).
14. S. V. Stepanova, A. A. Polukhin, and A. V. Kostyleva, "Hydrochemical structure of waters in the eastern part of the Laptev Sea in the autumn of 2015," *Okeanologiya* (Moscow) **57**, (2017).
15. I. N. Sukhanova, M. V. Flint, E. Yu. Georgieva, et al., "Structure of phytoplankton communities in the eastern part of the Kara Sea," *Okeanologiya* (Moscow) **57**, (2017).
16. O. V. Shishkina, *Geochemistry of Marine and Ocean Silt Waters* (Nauka, Moscow, 1972) [in Russian].
17. J. Greinert and A. Derkachev, "Glendonites and methane-derived Mg-calcites in the Sea of Okhotsk, Eastern Siberia: implications of a venting-related ikaite/glendonite formation," *Mar. Geol.* **204**, 129–144 (2004).
18. L. A. Kodina, V. G. Tokarev, L. N. Vlasova, and G. S. Korobeinic, "Contribution of biogenic methane to ikait formation in the Kara Sea: evidence from the stall carbon isotope geochemistry," *Proc. Marine Sci.* **6**, 349–374 (2003).
19. L. A. Kodina, V. G. Tokarev, L. N. Vlasova, and T. N. Pribylova, "Carbonate minerals ikaite and glendonite carbonate nodules in Holocene Kara Sea sediments: geological and isotopic evidence," *Rep. Pol. Mar. Res.* **393**, 189–196 (2001).
20. V. M. Kuptsov and A. P. Lisitzin, "Radiocarbon of Quaternary along shore and bottom deposits of the Lena River and the Laptev Sea sediments," *Mar. Chem.* **53**, 301–311 (1996).
21. H. Pauly, "Ikait", a new mineral from Greenland Arctic," *Arctic* **16** (4), 263–264 (1963). doi 10.14430/arctic3545
22. C. J. Schubert, D. Nürnberg, N. Scheele, et al., " ^{13}C isotope depletion in ikaite crystals: evidence for methane release from the Siberian shelves?" *Geo-Mar. Lett.* **17**, 169–174 (1997).
23. D. J. Shearman, A. McGugan, C. Stein, and A. J. Smith, "Ikait", $\text{CaCO}_3 \cdot 6\text{H}_2\text{O}$, precursor of the thinolites in the Quaternary tufas and tufa mounds of the Lahontak and Mono Lake basins, western United States," *GSA Bull.* **101**, 913–917 (1989).
24. E. Suess, W. Balzer, K.-F. Hesse, et al., "Calcium carbonate hexahydrate from organic-rich sediments of the Antarctic shelf: precursors of glendonites," *Science* **216**, 1128–1131 (1982).
25. E. Taldenkova, H. A. Bauch, A. Stepanova, et al., "Postglacial to Holocene history of the Laptev Sea shelf as reflected in molluscan, ostracodal, and foraminiferal faunas," *Global Planet. Change*, No. **4**, 223–251 (2005).
26. J. A. Welhan and Y. E. Lupton, "Light hydrocarbon gasses in Guaymas Basin hydrothermal fluids: thermogenic versus abiogenic origin," *Am. Assoc. Petrol. Geol. Bull.* **71**, 215–223 (1987).

Translated by N. Kravets